Texas A&M University
Mechanical Engineering Department
Turbomachinery Laboratory

Predictions vs. Test Results for Leakage and Rotordynamic Force Coefficients of a Fully Partitioned Pocket Damper Seal and a Labyrinth Seal - Limitations of the Current Computational Model

Research Progress Report to Turbomachinery Research Consortium
TRC-SEAL-02-13

By

Weilian Shan
Research Assistant

Luis San Andrés
Mast-Childs Professor

May 2013

TRC Project:
Engineering Analyses for Gas Pocket Damper Seals and Combined Labyrinth-Brush Seals

Predictions vs. Test Results for Leakage and Rotordynamic Force Coefficients of a Fully Partitioned Pocket Damper Seal and a Labyrinth Seal - Limitations of the Current Computational Model

Executive Summary

Pocket damper seals (PDS) evolved from labyrinth seals (LS) by adding radial baffles between pairs of blades, thus dividing the circumferential plenum into pockets of equal arcuate length, whose role is to brake the evolution of the circumferential flow velocity. A PDS leaks more than a LS, but the PDS provided a lot more effective damping and attenuate rotor vibration amplitudes more efficiently than a LS.

The technical report gives introduction to the program TAMU PDSeal and the user interface XLPDS®. Also, this report delivers predictions of rotordynamic force coefficients for a test LS and a test FPDS in Ref. [1]. The predicted rotordynamic force coefficients correlate well with the test data for the labyrinth seal [1]. However, predicted force coefficients for the FPDS are in gross error when compared to the experimental coefficients. Hence, the current computational program shows severe limitations to predict the dynamic force performance of PDSs with thick walls.

The physical model in the TAMU PDSeal program is a one-control volume, turbulent bulk flow model that includes the effects of circumferential flow velocity within a seal pocket and uses Neumann's leakage equation across the seal blades. The model ignores the flow resistance along the circumferential direction, badly needed for PDS with blunt blades of sizable axial thickness. Needless to state that, it is in this region the seal develops a cross-coupled stiffness as the gas is whirled because of shaft rotation. Recommendations for modifications of the PDSeal code are given at the end of this report.

Predictions vs. Test Results for Leakage and Rotordynamic Force Coefficients of a Fully Partitioned Pocket Damper Seal and a Labyrinth Seal - Limitations of the Current Computational Model

Table of Contents

List of Tables

List of Figures

Nomenclature

A_i	$L(B+H)$ Cross-section area between seal and shaft of the i^{th} control volume [m^2]
B	Seal teeth height [m]
C, c	Seal direct / cross-coupled damping force coefficients [N-s/m]
C_f	Flow contraction coefficient [-]
C_k	Kinetic energy carryover coefficient [-]
d	Cavity depth [m]
D_d	$2L(B+H)/(L+B+H)$ Hydraulic diameter [m]
e	Surface roughness [m]
H	Seal clearance [m]
h	Nominal clearance [m]
K, k	Seal stiffness force coefficients [N/m]
L	Axial length of seal cavity [m]
$\dot{M}$	Axial mass flow rate [kg/s]
$\dot{m}$	Axial mass flow rate per unit circumferential length [kg/m/s]
n	Number of teeth
P_i	Pressure in the i^{th} cavity [Pa]
P_{in}	Supply pressure [Pa]
P_{out}	Back pressure [Pa]
R_g	Specific gas constant [J/kg/K]
R_a	$\frac{1}{2}(R_L + R_s)$ Average seal radius [m]
R_r	Rotor radius [m]
Re	Reynolds number
s_i	Distance between the centers of the i^{th} and the $i+1^{th}$ cavities [m]
T	Temperature [K]
t	Time [s]
t_b	Blade tip thickness [m]
U	Circumferential bulk-flow velocity in seal pocket [m/s]
V	Axial velocity [m/s]
γ	Specific heat ratio [-]
μ	Fluid viscosity [Pa-s]

Ω	Journal rotation speed [rad/s]
ω	Excitation frequency [Hz]

A Short literature review on pocket damper seals

Labyrinth seals (LS) are installed in compressors and turbines as balance piston drums, interestage seals and impeller seals to prevent fluid leakage from a high pressure region to a low pressure region [2]. The blades (teeth) of a LS are very sharp and act as orifice-like restrictions resisting the axial flow. LSs are effective in restricting leakage [3]; however, experimental results [4, 5] evidence two disadvantages of LSs. One is that the direct damping coefficient of a LS is usually small, even negative; and the other disadvantage is that the evolution of the circumferential flow velocity along the seal causes large cross coupled stiffnesses, which are known drivers of rotor-bearing system instability. Hence, LSs provide limited effective damping and could even act to destabilize a whole rotor bearing system. [6]

Pocket damper seals (PDS) evolved from labyrinth seals by adding radial baffles between pairs of blades, thus dividing the circumferential plenum into pockets of equal arcuate length. The baffles role is to brake the evolution of the circumferential flow velocity. Early experiments [6, 7] were conducted to reveal the effectiveness of amplitude of imbalance response well in reducing in a rotor with the seals installed mid plane. Test results show a PDS leaked more than a LS [7], but the PDS provided a lot more effective damping (100 times more) and attenuated rotor vibration amplitudes more efficiently than a LS [6].

In 1993 Vance and Shultz [6] conducted experimental measurements in a non-rotating shaft and with a two-bladed four-pocket PDS with diverging clearance. The blades of the PDS were as sharp edged as those in a typical LS. The test results show the PDS has more than fifteen times damping than that in a conventional LS with the same clearance, and while operating with a pressure ratio (supply pressure / discharge pressure) equal to 3.1 [6].

In 1996 Vance and Li [7] conducted further experiments in a rotating shaft and with the same PDS as in Ref. [6]. The authors report the leakage of the PDS is about 30% higher than that of a conventional LS both with the same dimensions and operating under identical conditions. In addition, the leakage of both the PDS and the LS increase linearly with the pressure ratio (supply pressure / back pressure = ambient pressure). However, the leakage of the PDS increases faster than that of the LS when the pressure ratio increases [7]. At the time (1993-1996), the measurements were a revelation of the potential impact PDSs could have in commercial rotating machinery.

Bulk-flow models [8] are typically used to predict the leakage and the rotordynamic force coefficients of LSs. Li and San Andrés [9] apply the bulk-flow model [8] in a one control volume (1CV) method to predict the leakage and rotordynamic force coefficients in a single cavity PDS with two sharp teeth. As compared to a simple lumped parameter model [10], Li and San Andrés add the effects of fluid viscosity, flow turbulence, and circumferential flow swirl velocity within a seal pocket. The wall shear stress differences are functions of the local flow Reynolds number and rotor/stator surface conditions. Neumann's empirical leakage model [11] is used for prediction of the axial mass flow rate though a tooth clearance.

Li and San Andrés [9] also report predicted mass flow rate and direct damping coefficient for a two-bladed, four-pocket PDS with sharp teeth that correlate well with the test data in Ref. [12]. Li *et al.* [13] make further comparisons between predictions and test results for the rotordynamic force coefficients and the leakage flow rate of a two-bladed, four-pockets PDS of diverging clearance. The experiments and predictions show that the direct stiffness, damping force coefficients and leakage flow rate of the PDS are weak functions of rotor speed and proportional to the pressure ratio (supply pressure/discharge pressure). The test results do not

show an apparent trend for the cross-coupled stiffnesses versus rotor speed while the numerical prediction estimates that the cross-coupled stiffnesses slightly increase. The magnitudes of both measured and predicted cross-coupled stiffness coefficients are much smaller than that of the direct stiffness coefficients. The 1-CV bulk-flow model correctly predicts a negative direct stiffness coefficient and a large positive direct damping coefficient. Both the predictive model and the experiments show that the seal leakage increases as the pressure ratio increases. However, using Neumann's leakage model [11] slightly over-predicts the leakage (4-10%) compared with the test results in Ref. [12]. Li *et al.* [13] find similar conclusions from further experiments and comparisons with the predictions in Ref. [14].

The blades (teeth) of LS are very sharp so that the regions between the teeth and the rotor are modeled just as orifices without considering the blade thickness. Predicted force coefficients and leakage of a PDS with sharp teeth correlate well with the test data in Ref. [9, 13] by using the same bulk-flow 1-CV model as LS.

In an effort to quantify accurately leakage in PDSs and see-through LSs, Gamal [15] evaluates the accuracy of thirteen flow models, as listed in Table 1, against test data from Picardo [16] for a LS, and from Gamal [17] and Ertas [18] for PDSs. The various equations differ in their fundamental of physics, kinetic energy carryover coefficients (C_k) and flow constrain coefficients (C_f).

Table 2 lists the three typical gas leakage equation models used in LS analysis. There are St. Venant's, Martin's, and Neumann's basic leakage equation. Ref [15] implements the three fundamental gas leakage equations considered with three kinetic energy carryover coefficients (C_k) as listed in Table 3 (Hodkinson, Neumann, and Vermes) and two flow contraction

coefficients (C_f) as listed in Table 4 (Chaplygin's geometry dependent value [19] and Esser and Kazakia constant value [20]), to make the fourteen different leakage models listed in Table 1.

Table 1. Summary of leakage models [15]

Model	Basic gas leakage equation	Kinetic Energy Carryover Coefficient (C_k)	Flow Contraction Coefficient (C_f)
St. Venant	St. Venant	None	None
Martin	Martin	None	Constant
Hodkinson	Martin	Hodkinson	Empirical
Vermes	Martin	Vermes	Empirical
Neumann	Neumann	Neumann	Chaplygin
Zimmerman & Wolf	St. Venant & Martin	Empirical	Empirical
Esser & Kazakia	Neumann	Esser & Kazakia	Constant
Scharrer	Neumann	Vermes	Chaplygin
MOD.1	St. Venant	Hodkinson	None
MOD.2	St. Venant	Vermes	None
MOD.3	St. Venant	Vermes	Chaplygin
MOD.4	Neumann	Vermes	None
MOD.5	St. Venant	Hodkinson	Chaplygin
Gamal model	St. Venant	Hodkinson	Constant

Table 2. Basic gas leakage equations through a restriction [15]

Neumann gas basic leakage equation	St. Venant gas basic leakage equation	Martin gas basic leakage equation
$\dot{M}_i = C_{fi} C_{fi} A_i \sqrt{\frac{P_i^2 - P_{i+1}^2}{R_g T}}$	$\dot{M}_i = C_{fi} C_{fi} \frac{P_i A_i}{\sqrt{R_g T}} \sqrt{\frac{2\gamma}{\gamma - 1}\left[1 - \left(\frac{P_{i+1}}{P_i}\right)\right]}$	$\dot{M}_i = C_{fi} C_{ki} \frac{A P_{in}}{\sqrt{R_g T}} \sqrt{\frac{1 - \left(\frac{P_{out}}{P_{in}}\right)^2}{n - \ln\left(\frac{P_{out}}{P_{in}}\right)}}$

where $\dot{M}_i$ is the axial flow rate at the i^{th} tooth [kg/s], A_i is the clearance area under the i^{th} tooth, and P_i is the pressure in the i^{th} cavity, P_{in} is the supply pressure, P_{out} is the back pressure, n is the number of teeth, R_g is the specific gas constant, T is the temperature, and g is the specific heat ratio.

Table 3. Kinetic energy carryover coefficient (C_k) for leakage equations through a restriction [15]

Hodkinson	Neumann	Vermes
$C_{ki} = \sqrt{\dfrac{1}{1-\left(\dfrac{n-1}{n}\right)\cdot\left(\dfrac{H_i/L_i}{H_i/L_i+0.02}\right)}}$	$C_{ki} = \sqrt{\dfrac{n}{n\cdot(1-\alpha_i)+\alpha_i}}$ $\alpha_i = 1-\dfrac{1}{\left(1+16.6\dfrac{H_i}{s_i}\right)^2}$	$C_{ki} = \sqrt{\dfrac{1}{1-\alpha_i}}$ $\alpha_i = \dfrac{8.52}{\dfrac{s_i-t_i}{H_i}+7.23}$

n is the number of teeth, H_i is the clearance of the i^{th} tooth, L_i is the length of the i^{th} cavity, t_i is the blade tip thickness of the i^{th} tooth, s_i is the distance between the centers of the i^{th} and the $(i+1)^{th}$ cavities

Table 4. Flow contraction coefficient (Cf) for leakage equations through a restriction [15]

Chaplygin	Constant
$C_{fi} = \dfrac{\pi}{\pi+2-5\beta_i+2\beta_i^2}$ $\beta_i = \left(\dfrac{P_i}{P_{i+1}}\right)^{\gamma-1/\gamma} - 1$	$C_{fi} = 0.716$

P_i is the pressure in the i^{th} cavity, n is the number of teeth , and g is the specific heat ratio.

A leakage model using either St. Venant's equation or Neumann's equation iteratively calculates the pressure drop in consecutive cavities of a seal from upstream to downstream region. A leakage model using Martin's equation simply uses the total number of teeth (n), supply pressure (P_{in}) and back pressures (P_{out}) to calculate the seal leakage. Hence, leakage models using Martin's equation do not require or provide any information on intermediate pressures. However, this can be circumvented by applying Martin's Equation to each individual cavity to compute intermediate pressures. [15]

Gamal [15] discovers that the examined leakage equations deliver results of varying accuracy. Vermes' Model and MOD.2 and MOD.4 listed in Table 1 produce the most accurate leakage predictions for high-pressure LSs, whereas the Neumann Equation, Scharrer Equation and Gamal MOD.3 predict leakage with high accuracy for low pressure LSs. St. Venant's, Martin's, Vermes' and Neumann's Equations reasonably predict the leakage rate of certain PDSs. [15]

Gamal [15] also finds that blade thickness produces a drag force on the flow. However, none of the evaluated models takes friction from the blades into account or accurately accounts for the effect of blade thickness. The blade thickness is only considered as a geometrical term in Vermes' kinetic carryover factor. Experimental results show the leakage reduces significantly as the blade thickness increases. Gamal concludes that the under-predicted leakage flow rate for high-pressure LSs is at least partially due to unknown effects from too thick blades [15].

Commercial PDSs have invariably thick teeth, not sharp blades. The thickness of a twelve-bladed PDS in Ref. [18] is 3.175 mm while the cavity widths are 5.283 mm and 3.175 mm, which are the same order of magnitude as the blade thickness. Ertas *et al.* [1] recently compare the rotordynamic force coefficients of a fully partitioned damper seal (FPDS), a LS and a honeycomb seal (HC) operating with a high pressure ratio of 6.9 over a frequency range from 25 Hz to 250 Hz. FPDSs have axial baffles covering the whole seal axial extent and the pockets are separated by thick small clearance regions, which can amount to 20% of the whole sealing area. The blade thickness of the test FPDS is 3.175 mm and the baffle thickness is 3.556 mm, which cannot be regarded as sharp (rather blunt) compared with the pocket cavity axial length, 6.35 mm or 13.97 mm. Also, the empirical leakage equation cannot be used because there is an

axial pressure change along the "blade". A new 1CV bulk-flow model that includes the axial flow momentum is needed to obtain more accurate predictions.

Sheng *et al.* [21] recently measured the leakage of two fully-partitioned PDS (FPDS) with different cavity depths, a honeycomb seal (HS) and a LS. All four seals have the same nominal clearance ($H = 0.292mm$), operate at 15,000 rpm rotor speed, and operate with a range of inlet pressures from 6.9 bar to 20.7 bar (pressure ratio from 1.15 to 2.15). Test results show that the FPDS leaks 9-21% more than those from the LS and HC do, and a FPDS with a smaller cavity depth ($d = 3.175mm$) leaks less than the FPDS does with a larger cavity depth ($d = 6.175mm$) [21]. The authors indicate that the leakage performance of PDS can be improved by optimizing certain seal geometry parameters like decreasing the cavity depth.

This technical report provides predictions for the leakage and rotordynamic force coefficients of a LS and a PDS with thick walls using the TAMU PDSeal code which is strictly valid for LSs and PDSs with sharp teeth. Recommendations for modifications of the PDSeal code are also given at the end of this report.

Main features in bulk-flow model [22] and the TAMU PDSeal code

Ref. [22] by Li and San Andres details analysis of PDS with a 1-CV bulk-flow model. The TAMU PDSeal program solves the main flow continuity equation, circumferential momentum equation and Neumann's leakage mode. The program performs a small amplitude motion perturbation analysis to calculate the rotordynamic force coefficients. Table 5 sums the major features of the TAMU PDSeal code, as designed for PDSs and FPDSs with sharp teeth (blades).

Table 5 Summary of main features of TAMU PDSeal code

Governing Equations	Continuity equation, circumferential momentum equation in pockets
wall Stress	Moody's friction formulas
Leakage model (blades)	Neumann model
Ideal gas assumption	$\rho = P / R_g T$
Perturbation Analysis	Non-synchronous solution (excitation frequency)
Teeth Location	On stator
Multiple Case Variables	Rotor speed, excitation frequency, supply and discharge pressure

Li [22] uses the Neumann's leakage model,

$$\dot{m}_i = \frac{(C_k C_f H)_i}{V_*^2} \sqrt{P_{i-1}^2 - P_i^2} \tag{1}$$

where C_k and C_f are kinetic energy carryover coefficient and flow contraction coefficient, respectively. P is the pressure, and U is the circumferential flow velocity.

The equation for main flow continuity and circumferential momentum in a pocket cavity are,

$$\frac{1}{R_g T}\left[\frac{\partial (PA)_i}{\partial t} + \frac{\partial (PAU)_i}{R_a \partial \Theta}\right] + \zeta_r (\dot{m}_{i+1} - \dot{m}_i) = 0 \tag{2}$$

$$\frac{1}{R_g T}\left[\frac{\partial (PAU)_i}{\partial t} + \frac{\partial (PAU^2)_i}{R_a \partial \Theta}\right] + \zeta_r (\dot{m}_{i+1} U_i - \dot{m}_i U_{i-1}) = -\frac{A_i}{R_a}\frac{\partial P_i}{\partial \Theta} + \Delta \tau_{xi} \tag{3}$$

$\dot{m}_i$ and $\dot{m}_{i+1}$ are the axial mass flow rates per unit circumferential length across the upstream tooth and downstream tooth of the ith cavity. A_i is the cross-section area in the ith axial cavity. The coefficient $\zeta_r = (R_r / R_a)$ accounts for the effect of the pocket depth when the volume of the differential control-volume is calculated with R_a, the average radius of the seal.

Li [22] uses Moody friction factor model to calculate the wall shear stresses differences,

$$\Delta\tau_{xi} = -\frac{\mu L_i}{D_d H_i}\left[k_{xi}U_i - k_{Ji}\frac{\Omega R_r}{2}\right] \tag{4}$$

where μ is the gas viscosity, L_i is the length of the i^{th} cavity, D_h is the hydraulic diameter, H_i is the clearance of i^{th} tooth, , Ω is the rotor speed and R_r is the rotor radius, k_{xi} and k_{Ji} are turbulent shear flow parameters,

$$\begin{aligned} k_{Ji} &= \zeta_r k_{ri}, \qquad k_{xi} = \frac{\zeta_r k_{ri}}{2} + \frac{1}{2}\left(\frac{\zeta_s L_i + B_i + B_{i+1}}{L_i}\right)k_{si} \\ k_{ri} &= f_{ri}\,\mathrm{Re}_i, \qquad k_{si} = f_{si}\,\mathrm{Re}_i \end{aligned} \tag{5}$$

The Moody's friction factor equals

$$f = M_1\left\{1+\left[\frac{10^4 e}{B+H} + \frac{M_2}{\mathrm{Re}}\right]^{M_3}\right\} \tag{6}$$

$$M_1 = 1.375\times10^{-3}, M_2 = 1\times10^6, M_3 = \frac{1}{3} \tag{7}$$

where e is the surface roughness and Re is the local Reynolds number, $\mathrm{Re} = \frac{\rho}{\mu}h\sqrt{U^2+V^2}$

Li [22] solves for non-synchronous shaft motion by input of excitation frequencies and rotor speed to the TAMU PDSeal code with a Bulk-Flow model as in Childs [23] who uses a bulk-flow version of the Navier-Stokes equations. The seal linearized reaction force is $x = (X,Y)^T$ about a centered position as

$$-\begin{Bmatrix} F_X \\ F_Y \end{Bmatrix} = \begin{bmatrix} K & k \\ -k & K \end{bmatrix}\begin{Bmatrix} X \\ Y \end{Bmatrix} + \begin{bmatrix} C & c \\ -c & C \end{bmatrix}\begin{Bmatrix} \dot{X} \\ \dot{Y} \end{Bmatrix} \tag{8}$$

where K, C are the direct stiffness and damping coefficients, and k, c are the cross coupled stiffness and damping coefficients. A zero order solution gives the steady-state pressure field, the circumferential velocity field and the seal leakage. Solution to first order equations gives pressure field to determine the rotordynamic force coefficients.

Introduction to XLPDS® worksheet

During 2013, a GUI was created to run the TAMU PDSeal automatically. XLPDS® Worksheet, as shown in Figure 1 (a)-(d), provides a convenient way for a user to predict the leakage and the force coefficients and of a gas pocket damper seal (PDS), or a fully partitioned damper seal (FPDS).

The users need to input the seal geometry and operating conditions see Figure 1. XLPDS® can perform multiple predictions by inputting multiple sets of supply pressure, discharge pressure, rotor speed and excitation frequency, as shown in Figure 1 (c). The code outputs force coefficients and leakage, as shown in Figure 1 (d).

The active / inactive blades are blades without / with a notch. A seal with staggered pocket damper cavities and labyrinth seal cavity is a traditional PDS. A seal with all cavities as pocket damper is a fully-partitioned damper seal.

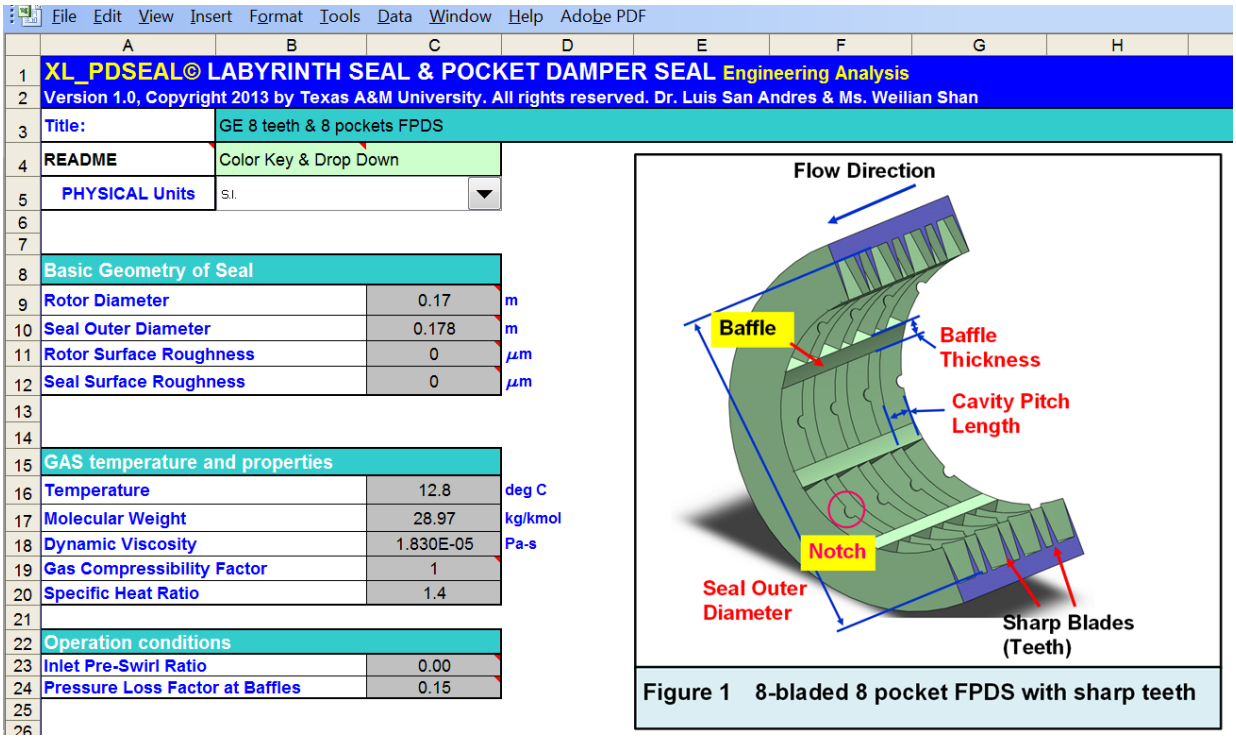

Figure 1 (a) GUI XLPDS® Worksheet for PDS and FPDS: input parameters

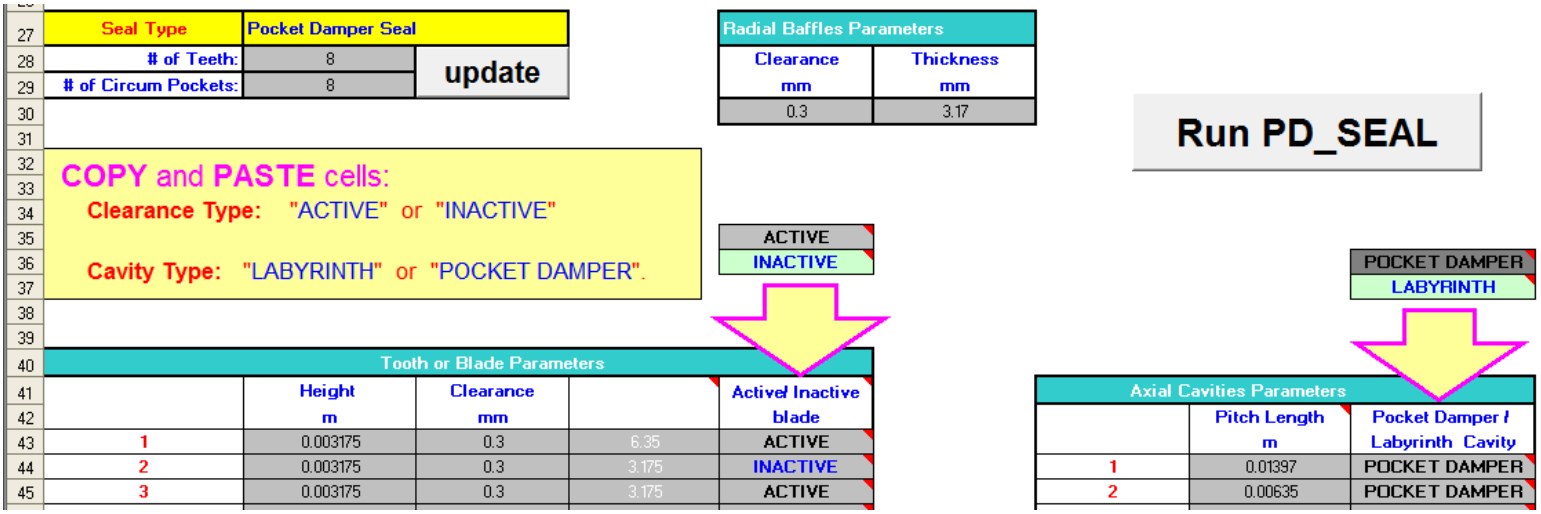

Seal Type	Pocket Damper Seal	
# of Teeth:	8	update
# of Circum Pockets:	8	

Radial Baffles Parameters	
Clearance mm	Thickness mm
0.3	3.17

Run PD_SEAL

COPY and PASTE cells:
Clearance Type: "ACTIVE" or "INACTIVE"
Cavity Type: "LABYRINTH" or "POCKET DAMPER".

ACTIVE
INACTIVE

POCKET DAMPER
LABYRINTH

Tooth or Blade Parameters				
	Height m	Clearance mm		Active/ Inactive blade
1	0.003175	0.3	6.35	ACTIVE
2	0.003175	0.3	3.175	INACTIVE
3	0.003175	0.3	3.175	ACTIVE

Axial Cavities Parameters		
	Pitch Length m	Pocket Damper / Labyrinth Cavity
1	0.01397	POCKET DAMPER
2	0.00635	POCKET DAMPER

Figure 1 (b) GUI XLPDS® Worksheet for PDS and FPDS : more input parameters

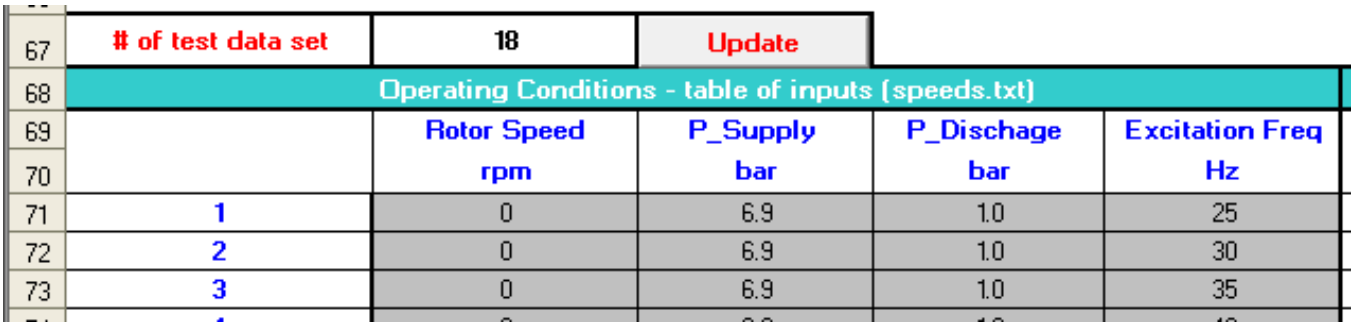

# of test data set	18	Update		
Operating Conditions - table of inputs (speeds.txt)				
	Rotor Speed rpm	P_Supply bar	P_Dischage bar	Excitation Freq Hz
1	0	6.9	1.0	25
2	0	6.9	1.0	30
3	0	6.9	1.0	35

Figure 1 (c) GUI XLPDS® Worksheet for PDS and FPDS: table of operating conditions

Force Coefficient								Results
Kxx N/m	Kxy N/m	Kyx N/m	Kyy N/m	Cxx N-s/m	Cxy N-s/m	Cyx N-s/m	Cyy N-s/m	Leakage kg/s
-6.682E+06	8.062E-02	-8.062E-02	-6.682E+06	1793	-2.6410E-05	2.6410E-05	1793	0.1046
-6.637E+06	8.257E-02	-8.257E-02	-6.637E+06	1785	-2.6740E-05	2.6740E-05	1785	0.1046
-6.587E+06	8.463E-02	-8.463E-02	-6.587E+06	1777	-2.7100E-05	2.7100E-05	1777	0.1046

Figure 1 (d) GUI XLPDS® Worksheet for PDS and FPDS: predictions

Example of predictions

Ertas *et al.* [1] conduct experiments on a labyrinth seal (LS) and a fully partitioned damper seal (FPDS) and compare the identified rotordynamic force coefficients. Table 6 lists the dimensions of the tested LS and FPDS in Ref. [1], respectively. Table 7 lists the operating conditions given in Ref. [1]. Tests were conducted on a LS and a FPDS on a 170 mm diameter rotor for rotor speeds of 7,000 rpm and 15,000 rpm, with an inlet air pressure of 6.9 bar (absolute pressure), ambient back pressure (1.0 bar), inlet preswirl ratio of 0 and 0.96, and with excitation frequencies from 25 Hz up to 250 Hz.

Table 6 Dimensions of LS, FPDS and rotor [1]

	LS	FPDS
Number of blades	14	8
Number of pockets	1	8
Blades properties	All active	Active / Inactive (without notch / with notch)
Cavity depth	4 mm	3.175 mm
Cavity axial length	5.004 mm	13.97 mm (1, 3, 5, 7 cavity) 6.35 mm (2, 4, 6 cavity)
Blade axial length	0	6.35 mm (1 blade) 3.175 mm (2, 3, 4, 5, 6, 7, 8 blade)
Radial clearance	0.3 mm	0.3 mm
Seal overall length	65 mm	102.87 mm
Rotor Diameter	170 mm	170 mm

Table 7 Operating conditions for test seals in Ref. [1]

Inlet pressure		6.9 bar (absolute pressure)	
Back pressure (Atmosphere)		1 bar (absolute pressure)	
Excitation frequency		0 – 250 Hz	
Inlet temperature		285.93 K (12.78 °C)	
Rotor speed		7,000 rpm	15,000 rpm
Rotor surface velocity (ΩR)		62.3 m/s	133.5 m/s
Inlet preswirl velocity	0	60 m/s	
Preswirl ratio	0	0.96	0.45

Inlet preswirl ratio equals inlet circumferential flow speed divided by rotor surface velocity (ΩR)

Gas	Air
Molecular weight	28.97
Gas compressibility factor	1
Specific heat ratio	1.4
Viscosity	18 μPa·s at 13°C

Figure 2 depicts the schematic view of the FPDS and the LS in Ref. [1]. The fourteen-bladed LS and the FPDS have the same radial clearance throughout $H = 0.3mm$. The FPDS has eight blades (seven axial cavities) and eight circumferential pockets in each cavity. In addition, downstream blades of pocket dampers are notched to make the clearance diverge as shown in Figure 3 [1].

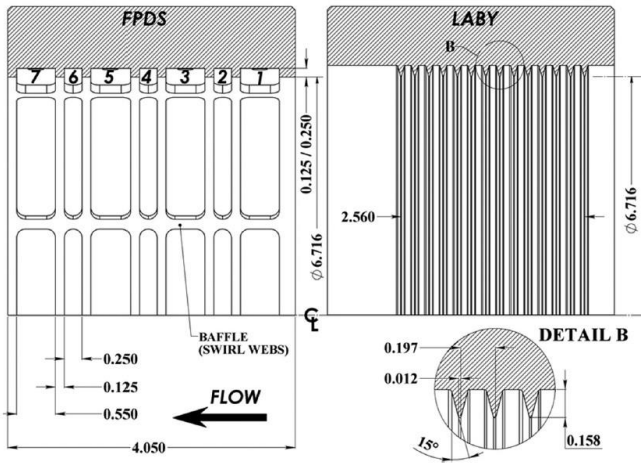

Figure 2 Schematic views of the tested FPDS and LS (in inches) [1]

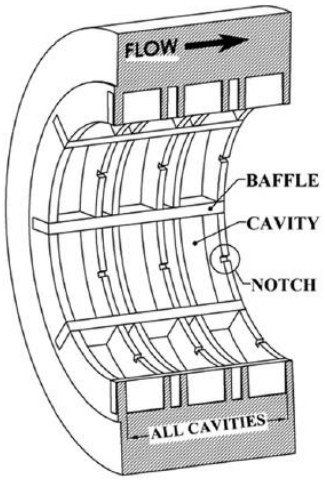

Figure 3 Schematic views of a six-bladed FPDS with notches on downstream blades [1]

Figures 4, 5 and 6 present the experimental results from the mechanical impedance testing on both FPDS1 and LS and predictions from the TAMU PDSeal code. For the test data, the direct coefficients are averages from in the *X* and *Y* directions.

Figure 4 shows the direct stiffness coefficients of the FPDS1 and LS versus excitation frequency at rotor speeds of 7,000 rpm and 15,000 rpm. Each graph includes both test results and predictions with inlet preswirl ratio = 0, 0.96 or 0.45. For the FPDS1, the direct stiffness from both test results and predictions increases as the excitation frequency increases. However, for the LS, the direct stiffness slightly decreases as the excitation frequency increases. The experimental direct stiffness of the FPDS1 is negative and small at low frequencies and then becomes positive at frequencies between 75 Hz and 100 Hz. On the other hand, the predicted direct stiffnesses for the FPDS1 are negative for all frequencies in the range of 25 Hz to 250 Hz. The absolute value of direct stiffness with preswirl is slightly higher than that without preswirl for both experimental results and predictions, except those predictions for an operating speed of 15,000 rpm and with a preswirl of 0.45. Rotor speed does not play a discernible role in affecting the direct stiffness for the test results. The experiments show direct stiffness coefficients of the LS are positive and minimal at low frequencies and become negative after the cross-over frequency. The cross-over frequency occurs between 125 Hz to 150 Hz. [1]

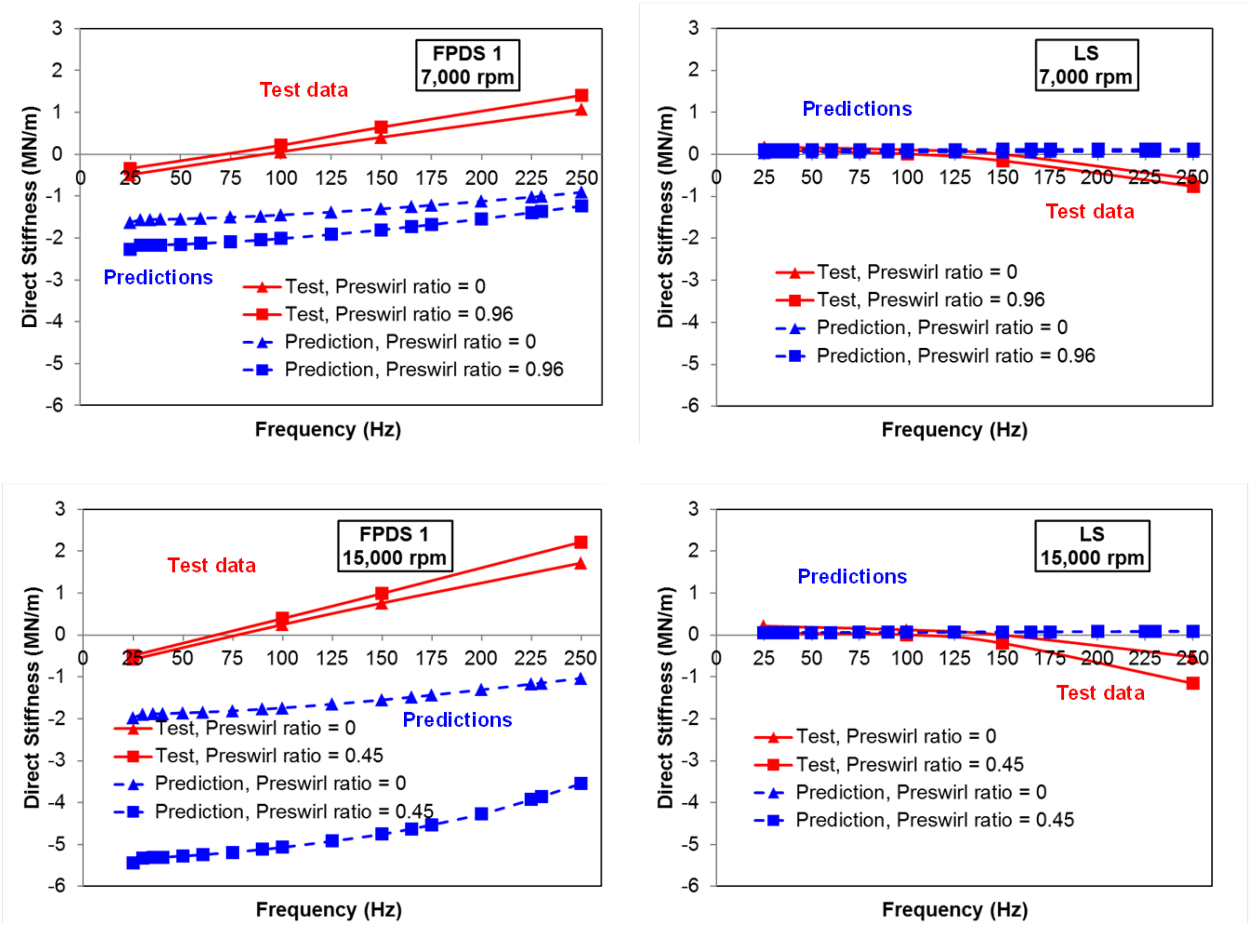

Figure 4 Direct stiffness coefficients of a FPDS1 and a LS versus excitation frequency. Rotor speeds = 7,000 rpm and 15,000 rpm. Preswirl ratios noted. Test data from Ref. [1]

Figure 5 depicts the direct damping coefficients of the FPDS1 and LS versus excitation frequency at rotor speeds of 7000 rpm and 15,000 rpm. Direct damping coefficient for LS is not sensitive to either rotor speed or excitation frequency; however, the direct damping coefficient for the FPDS decreases as the excitation frequency increases. Incidentally, the direct damping coefficient for the FPDS increases significantly (~20%) as the rotor speed increases [1].

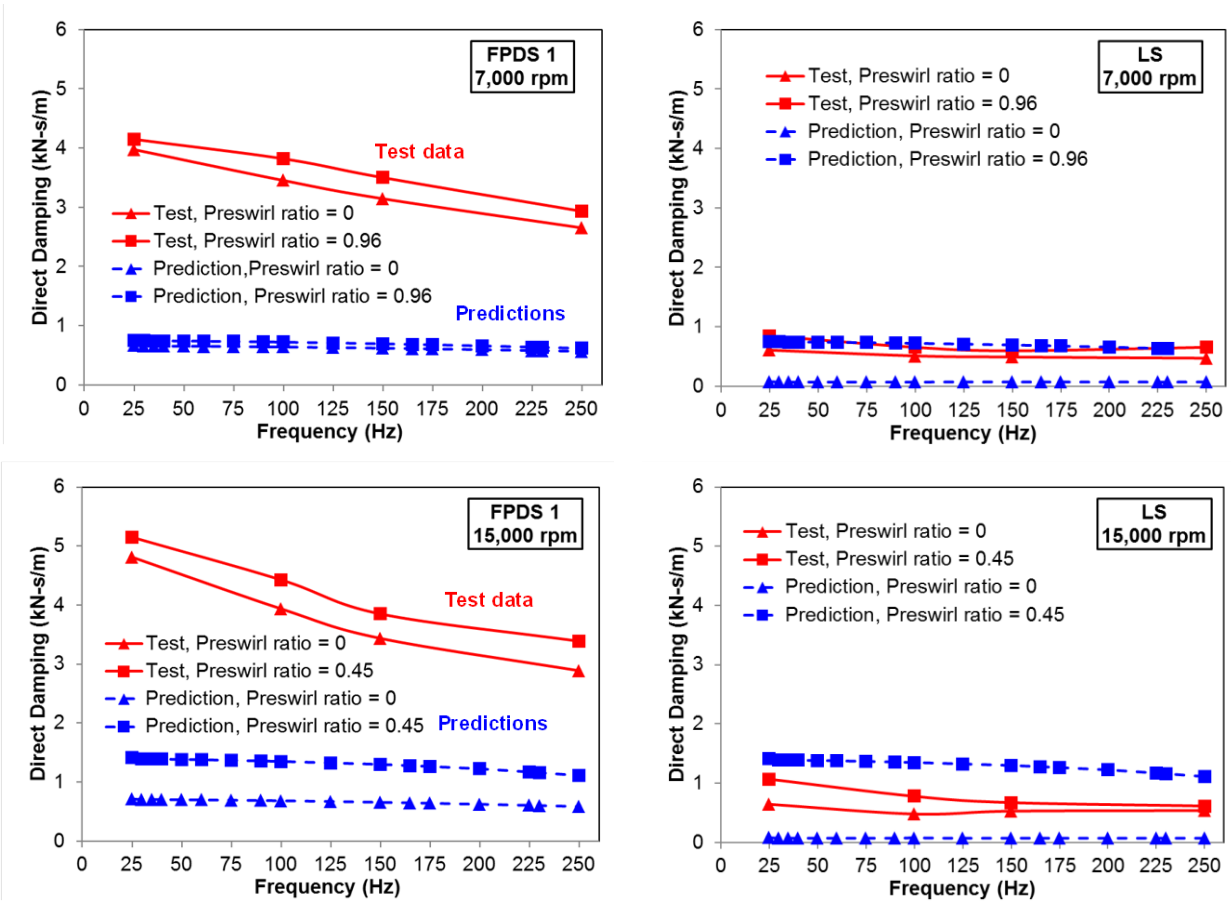

Figure 5 Direct damping coefficients of a FPDS1 and a LS versus excitation frequency. Rotor speeds = 7,000 rpm and 15,000 rpm. Preswirl ratios noted. Test data from Ref. [1]

Figure 6 shows the cross coupled stiffness versus excitation frequency. Rotor speed or excitation frequency does not influence the cross coupled stiffness. The cross coupled stiffnesses with an inlet preswirl are larger than those without preswirl.

Figures 4, 5 and 6 show that the predicted rotordynamic force coefficients correlate well with the test results for the LS, but the TAMU PDSeal code fails to provide reasonable predictions for the FPDS.

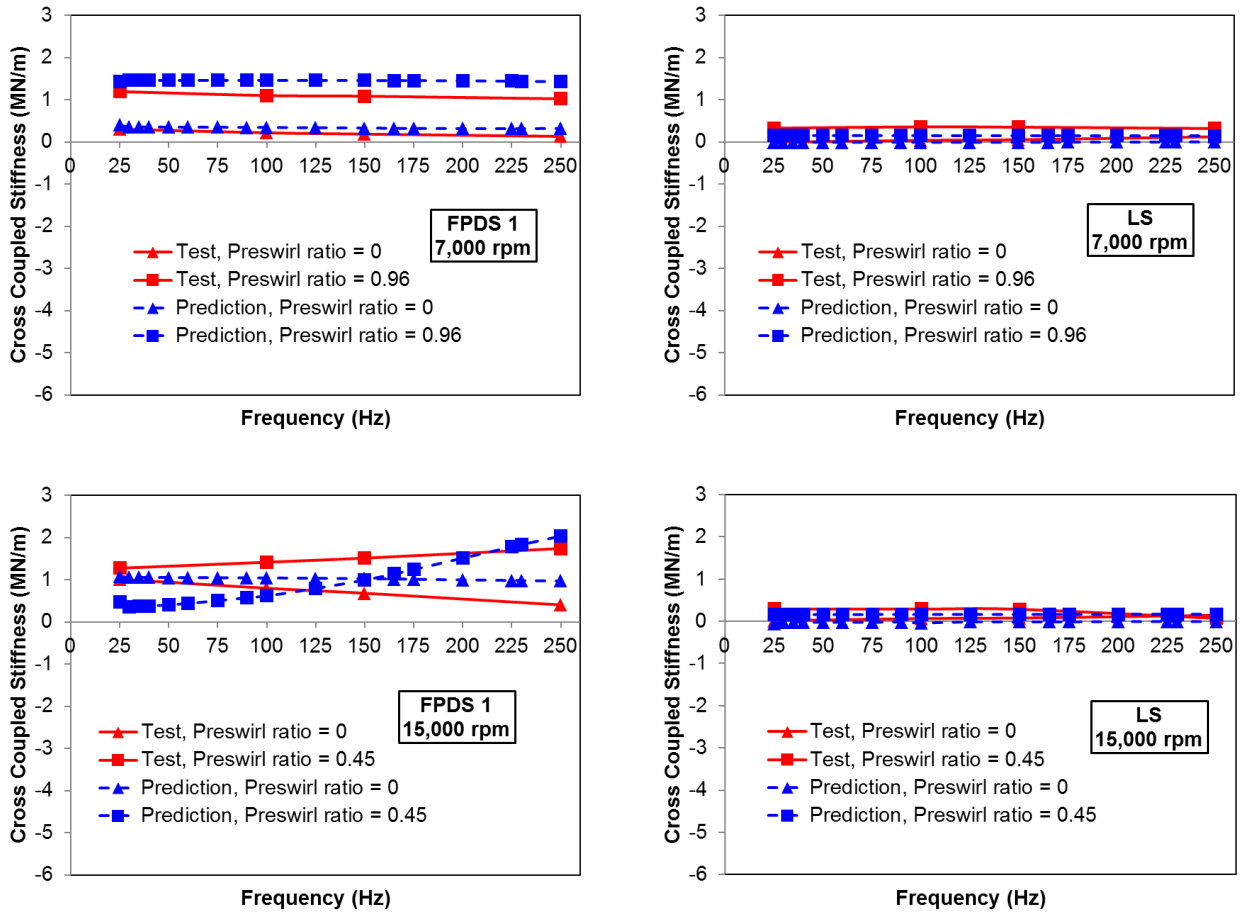

Figure 6 Cross coupled stiffness coefficients of a FPDS1 and a LS versus excitation frequency. Rotor speed = 7,000 rpm and 15,000 rpm, Preswirl ratios noted. Test data from Ref. [1]

Figure 7 shows the effective damping coefficients ($C_{eff\,X}, C_{eff\,Y}$) versus excitation frequency, the effective damping coefficients are defined as [2]:

$$C_{eff} = C - \frac{k}{\omega}$$

For the experimental data, the effective damping of the FPDS is much larger than that of the LS. The effective damping is positive over the range of 50 Hz to 250 Hz. However, the predicted effective damping coefficients are all negative for both the FPDS and a LS with preswirl.

Figures 4, 5, 6, and 7 show that the predictions from the program TAMU PDSeal correlate well with the test data for the LS, but the program cannot deliver good predictions for the FPDS.

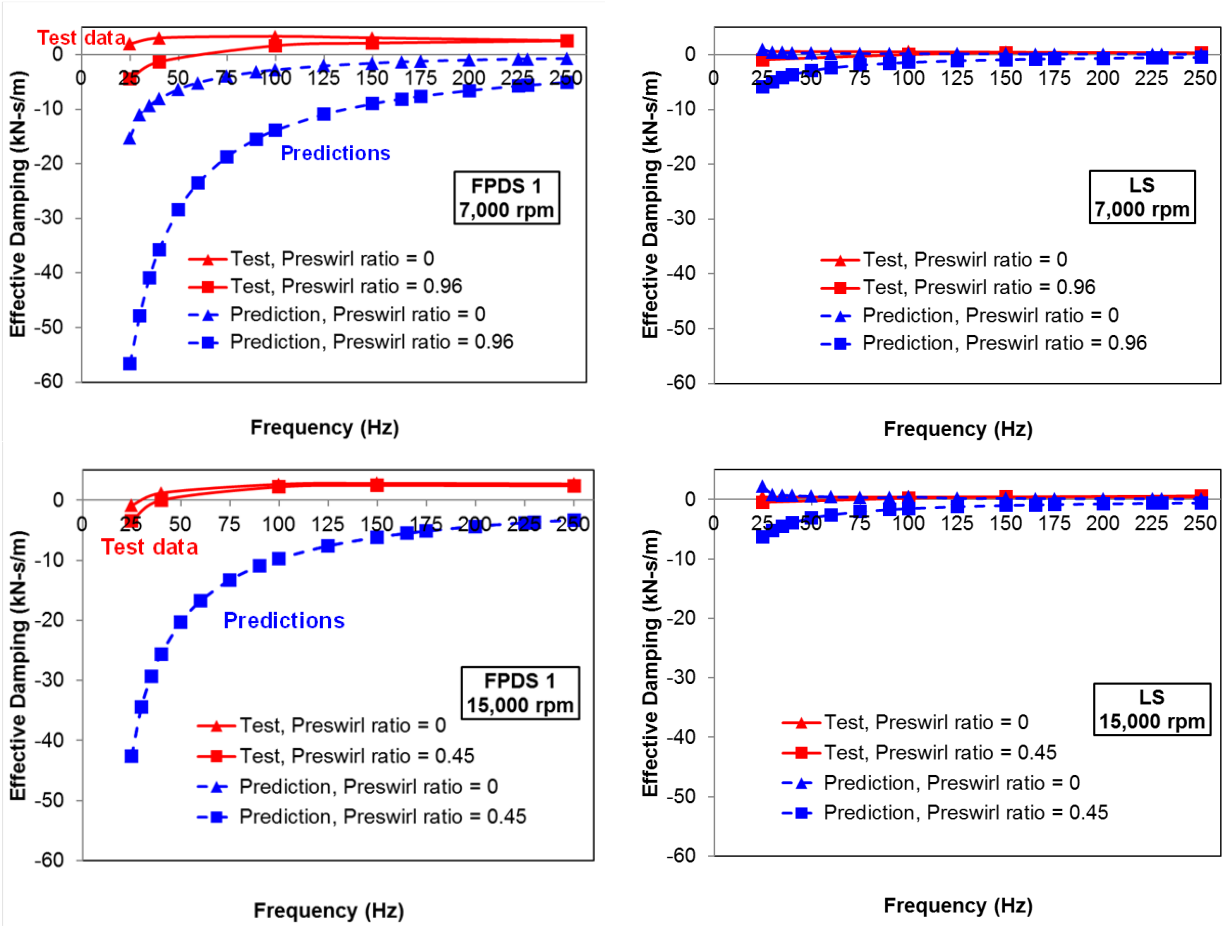

Figure 7 Effective damping coefficients of a FPDS1 and a LS versus excitation frequency. Rotor speeds = 7,000 rpm and 15,000 rpm. Preswirl ratios noted. Test data from Ref. [1]

Conclusions and recommendations

This report delivers predictions of rotordynamic force coefficients for a test LS and a test FPDS in Ref. [1]. The predicted rotordynamic force coefficients correlate well with the test data for the labyrinth seal [1]. However, predicted force coefficients for the FPDS are in gross error when compared to the experimental coefficients. Hence, the current computational program shows severe limitations to predict the dynamic force performance of PDSs with thick walls. The physical model in the TAMU PDSeal is a one-control volume, turbulent bulk flow model that includes the effects of circumferential flow velocity within a seal pocket and uses Neumann's leakage equation across the seal blades. The model ignores the flow resistance along the circumferential direction, badly needed for PDS with blunt blades of sizable axial thickness. Needless to state that, it is in this region the seal develops a cross-coupled stiffness as the gas is whirled because of shaft rotation.

For the further work, the specific tasks are:

- Update the physical model for PDS [9] by replacing the empirical leakage formulas with a bulk flow model that incudes flow conservation and circumferential and axial momenta transport equations in the flow region under a thick blade and the spinning rotor.
- Extend the bulk-flow model to include two-component mixtures (liquid in a gas) as in Ref. [26].

References

[1] Ertas, B.H., Delgado, A., Vannini, G., 2012, "Rotordynamic Force Coefficients for Three Types of annular Gas Seals with inlet Preswirl and High Differential Pressure ratio," ASME J. Eng. Gas Turbines Power, **134**, pp. 042503-1-12.

[2] Ransom, D., Li, J., San Andrés, L., and Vance, J., 1999, "Experimental Force Coefficients for a Two-Bladed Labyrinth Seal and a Four-Pocket Damper Seal," ASME J. Trib., **121**, pp. 370-376.

[3] Chupp, R. E., Hendricks, R. C., Lattime, S. B., and Steinetz, B. M., 2006, "Sealing in Turbomachinery," AIAA J. Propul. Power, **22**(2), pp. 313-349.

[4] Vance, J. M., Zierer, J. J., and Conway, E. M., 1993, "Effect of Straight-Through Labyrinth Seals on Rotordynamics," Proceedings of the ASME Vibration and Noise Conference, Albuquerque, New Mexico.

[5] Childs, D. W., and Scharrer, J. K., 1988, "Theory versus Experiment for the Rotordynamic Coefficients of Labyrinth Gas Seals, Part II – A Comparison to Experiment," J. Vibration, Acoustics, Stress, and Reliability in Design, **110**, July, pp. 281-287.

[6] Vance, J. M., and Schultz, R. R., 1993, "A New Damper Seal for Turbomachinery," ASME Vibration of Rotating Systems, DE **60**, pp. 139-148.

[7] Vance, J. M., and Li, J., 1996, "Test Results of a New Damper Seal for Vibration Reduction in Turbomachinery," ASME, J. of Engineering for Gas Turbines and Power, **118**, October, pp. 843-846.

[8] Hirs, G. G., 1973, "A Bulk-Flow Theory for Turbulence in Lubricant Films," ASME J. of Lubrication Technology, **95**, pp. 137-146.

[9] Li, J., San Andrés, L., and Vance, J., 1999, "A Bulk-Flow Analysis of Multiple-Pocket Gas Damper Seals," ASME J. Eng. Gas Turbines Power, **121**, pp. 355-363.

[10] Vance, J. M., Cardon, B.P., San Andrés, L.A., and Storace, A.F., 1993, "A Gas-Operated Bearing Damper for Turbomachinery", ASME J. Eng. Gas Turbines Power, **115**, pp. 383-389.

[11] Childs, 1993, *Turbomachinery Rotordynamics – Phenomena, Modeling & Analysis, Wiley-Interscience*, NY, USA, Chap. 4 & 5.

[12] Li, J., 1995, "The Effect of A New Damper Seal on Rotordynamics," MS Thesis, Texas A&M University, College Station, TX.

[13] Li, J., Ransom, D., San Andrés, L., and Vance, J., 1999, "Comparison of Predictions With Test Results for Rotordynamic Coefficients of a Four-Pocket Gas Damper Seal," ASME J. Trib., **121**, pp. 363-369

[14] Li, J., Aguilar, R., San Andrés, L., Vance, J. M., 2000, "Dynamic Force Coefficients of a Multiple-Blade, Multiple-Pocket Gas Damper Seal: Test Results and Predictions," ASME J. Trib., **122**, pp. 317-322.

[15] Gamal Eldin, A. M., 2007, "Leakage and Rotordynamic Effects of Pocket Damper Seals and See-Through Labyrinth Seals," Ph.D. Dissertation, Texas A&M University, College Station.

[16] Picardo, A. M., 2003, "High Pressure Testing of See-Through Labyrinth Seals," M.S. Thesis, Mechanical Engineering Department, College Station, TX.

[17] Gamal, A. M., 2003, "Analytical and Experimental Evaluation of the Leakage and Stiffness Characteristics, of High Pressure Pocket Damper Seals," M.S. Thesis, Mechanical Engineering Department, Texas A&M University, College Station, TX.

[18] Ertas, B. H., 2005, "Rotordynamic Force Coefficients of Pocket Damper Seals," Ph.D. Dissertation, Texas A&M University, College Station.

[19] Gurevich, M. I., 1965, *Theory of Jets in an Ideal Fluid*, Academic Press, New York, Chapter 6.

[20] Esser, D. and Kazakia, J. Y., 1995, "Air Flow in Cavities of Labyrinth Seals," International Journal of Engineering Science, **33** (15), pp. 2309-2326.

[21] Sheng, N., Ruggiero, E. J., Devi, R., Guo, J., and Cirri, M., 2011, "Experimental and Analytical Leakage Characterization of Annular Gas Seals: Honeycomb, Labyrinth and Pocket Damper Seals," ASME Turbo Expo, Vancouver, British Columbia, Canada.

[22] Li, J., 1999, "A Bulk-Fow Model of Multiple-Blade, Multiple-Pocket Gas Damper Seals," Ph.D. Dissertation, Texas A&M University, College Station.

[23] Thorat, M., Childs, D., 2009, "Predicted Rotordynamic Behavior of a Labyrinth Seal as Rotor Surface Speed approaches Mach 1" , Proceedings of ASME Turbo Expo, Orlando, Paper GT2009-59256.

[24] Kim, C. H., Childs, D. W., 1987, "Analysis for Rotordynamic Coefficients of Helically-Grooved Turbulent Annular Seals," ASME J. Trib., 109, pp. 136-143

[25] Nelson, C. C., 1987, "Comparison of Hirs' Equation with Moody's Equation for Determining Rotordynamic Coefficients of Annular Pressure Seals," ASME J. Trib., 109, pp. 144-148

[26] San Andrés, L., 2012, "Rotordynamic Force Coefficients of Bubbly Mixture Annular Pressure Seals," ASME J. Eng. Gas Turbines Power, **134**, p. 022503.

Appendix A 1-Control-Volume governing equations for grooved seals

The model by Li [22] will be remodeled to include thick blades. Figure 1 shows the schematic view of an annular seal with circumferential grooves. The governing equations for the fluid flow in grooved seals are based on both Hirs' bulk-flow theory [8] and Kim's analysis for helically-grooved annular seals [24].

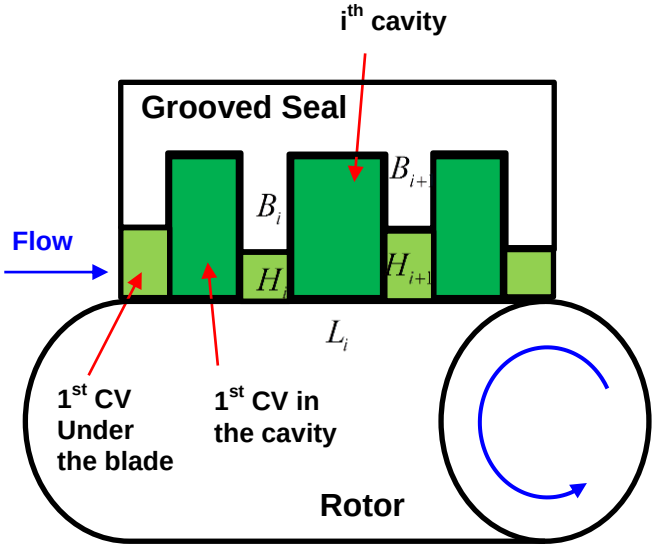

Figure 8 Schematic view of a circumferential grooved seal

Governing Equations for the i^{th} Cavity or for the land on the right of the i^{th} Cavity [24]

Continuity Equation [24]

$$\frac{L}{\xi_r}\frac{\partial(dP)_i}{\partial t}+\frac{\partial(HPV)_i}{\partial z}+\frac{\partial(dPU)_i}{R_r\partial\theta}=0 \tag{A1}$$

Circumferential Momentum Equation [24]

$$-\frac{1}{R_r}\tau_{\theta,i}-\frac{\partial(dLP)_i}{R_r\partial\theta}=\frac{1}{ZR_gT}\left[\frac{1}{\xi_r}\frac{\partial(dLPU)_i}{\partial t}+\frac{\partial(dLPU^2)_i}{R_r\partial\theta}+\frac{\partial(HLPUV)_i}{\partial z}\right] \tag{A2}$$

Axial Momentum Equation [24]

$$-\left[\frac{1}{R_r}\tau_{z,i}+\frac{\partial(HLP)_i}{\partial z}\right]=\frac{1}{ZR_gT}\left[\frac{1}{\xi_r}\frac{\partial(dLPV)_i}{\partial t}+\frac{\partial\left(HLPV^2\right)_i}{\partial z}+\frac{\partial(dLPUV)_i}{R_r\partial\theta}\right] \tag{A3}$$

Where
$$\xi_r=\frac{R_r}{R_a},\xi_s=\frac{R_s}{R_a} \tag{A4}$$

For the control volumes under blades, $\xi_r=\frac{R_r}{R_a}=1,\ \xi_s=\frac{R_s}{R_a}=1$

D is the depth of a control volume, $D=H+B$ for the control volumes in the cavities. $D=H$ for the control volumes under blades, i.e., $B=0$, B is the tooth height, and H is the clearance.

For fully developed turbulent flow, the wall shear stress differences in the circumferential direction and in the axial direction are [22]

$$\begin{aligned}\tau_{\theta,i}&=\tau_{s\theta,i}+\tau_{r\theta,i}=\frac{\mu R_a L_i}{D_i}\left[k_{Si}U_i-k_{Ri}\frac{R_r\Omega}{2}\right]\\ \tau_{zi}&=\tau_{rz,i}+\tau_{sz,i}=\frac{\mu R_a L_i}{D_i}k_{Zi}V_i\end{aligned} \tag{A5}$$

Where [22]

$$\begin{aligned}k_{Si}&=\frac{1}{2}\xi_r k_{ri}+\frac{L_i\xi_s+B_i+B_{i+1}}{2L_i}k_{si}\\ k_{Ri}&=\xi_r k_{ri}\\ k_{zi}&=\frac{1}{2}\xi_s k_{si}+\frac{1}{2}\xi_r k_{ri}\end{aligned} \tag{A6}$$

$$k_{ri}=f_r\,\mathrm{Re}_{ri},\quad k_{si}=f_s\,\mathrm{Re}_{si} \tag{A7}$$

The Reynolds numbers relative to the rotor (Re_{ri}) and the stator (Re_{si}) surfaces are [22]

$$\begin{aligned}\mathrm{Re}_{ri}&=\frac{\rho D_i}{\mu}\sqrt{(U_i-R_r\Omega)^2+V_i^2}\\ \mathrm{Re}_{si}&=\frac{\rho D_i}{\mu}\sqrt{U_i^2+V_i^2}\end{aligned} \tag{A8}$$

The friction factors are formulated using Moody's friction factor

$$f_x = 0.001375 \times \left[1 + \left(10^4 \frac{r_x}{H} + \frac{10^6}{\mathrm{Re}_x} \right)^{\frac{1}{3}} \right] \tag{A9}$$

Where x is either r (for the rotor) or s (for the stator), and r_x is the surface roughness.